Fluid Dynamics Research 11 (1993) 245–261
North-Holland

FLUID *DYNAMICS*
RESEARCH

Reconstruction of a quasi-instantaneous image of coherent structures from hotwire signals obtained by a multi-point simultaneous measurement system

Mikio Hino[#1]

Department of Civil Engineering, Tokyo Institute of Technology, 2-12-1, O-okayama, Meguro-ku, Tokyo 152, Japan

and

Yan Meng[#2]

Fluid Dynamics Group, Environmental Engineering Department, Institute of Technology, Shimizu Corporation, Etchujima 3-chome, Koto-ku, Tokyo 135, Japan

Received 16 December 1991
Accepted 3 November 1992

Abstract. The turbulent velocity components (u, v) at 11 points in a reciprocating oscillatory turbulent flow have been measured simultaneously by a set of eleven X-type hotwire probes located in a plane perpendicular to the mean flow. Using a conditional sampling technique and a new method of data analysis for the inverse estimation of flow fields called the "virtual plate/load and MASCON model", a quasi-instantaneous three-dimensional image of coherent structures of turbulence was first reconstructed directly from the experimental velocity data. The quasi-instantaneous image was expressed in terms of the velocity components u, v, w and the vorticity components $\omega_x, \omega_y, \omega_z$ and we found that the large-scale coherent structure was composed of a pair of counter-rotating fluid motions with asymmetry which was quite different from that of the ensemble-averaged one. Flow patterns induced by the large-scale structure have been clarified by perspective representations visualized by computer simulations that produce timelines and streaklines of fluid particle traces. Results showed that the new experimental method was applicable for investigating the three-dimensional feature of coherent structures including asymmetry.

1. Introduction

In 1959, Kline and Runstudler (1959) published their first paper, a rudimentary one prior to the epoch-making and pioneering paper by Kline and his colleagues (Kline, Reynolds, Schraub and Runstadler) published in 1967, which ignited the new era of turbulence research. They found that low-velocity lumps of fluid move away from the wall, in what was called coherent motion. Reviews on the recent developments in research on coherent structure are given, for instance, by Robinson (1991).

The three-dimensional feature of coherent motion in the intermittent region of a fully developed turbulent boundary layer was first disclosed experimentally by Fukunishi and Sato (1987a, b). They applied the conditional sampling technique under low-speed conditions; the

Correspondence to: Prof. M. Hino, Katase-Yama 4-20-6, Fujisawa-Shi, 251, Japan.
[#1] Present address: Faculty of Political Science, Chuo University, Higashi-Nakano 742-1, Hachiohji City, 192-03, Japan.
[#2] Formerly, Graduate Student at Tokyo Institute of Technology.

ensemble-averaged configuration they revealed is a pair of vortices aligned in the direction of the mean flow, which they called a "banana vortex". Unfortunately, as was perceived earlier and pointed out, for instance, by Hino et al. (1991), the conditional sampling and ensemble averages with one detector probe for investigating 3-D configurations of coherent motions have a fatal defect in that whole detected signals are averaged without proper discrimination except for a threshold condition, such as a threshold Reynolds stress or a threshold velocity. Consequently, the results obtained by hotwire measurements give a picture of a vortex pair symmetric with regard to the plane on which a detector probe is located, since vortices with different configurations such as asymmetric ones with stronger left and weaker right, or vice versa, will occur with uniform probability. Recently, asymmetric coherent structures have also been investigated by Antonia and Bisset (1989) using a new conditional averaging technique. It must also be pointed out that ensemble averages for data acquisition need too much time to investigate turbulence structures in the field-scale flows.

Flow visualization is also an efficient tool for obtaining a qualitative grasp of the features of the coherent structure. The method, however, sometimes leads to erroneous results because of incorrect interpretations, as experimenters using hot-wires have frequently pointed out. A visualized picture gives an integrated result of the flow field experienced by the tracer in the past (Hama, 1962).

Recently, the direct numerical simulation of the Navier–Stokes equation (Moin and Kim, 1982; Kim et al., 1987) has begun to yield images of coherent structures. Turbulence structures associated with the coherent motion envisaged by Kline et al. (1967) were investigated using data obtained from large-eddy simulation of turbulent channel flow by Kim (1985); he used the VITA technique (the variable-interval time-averaging technique) developed by Blackweder and Kaplan (1976) as the conditional sampling technique and exhibited the "splatting" motion during the sweep event and the existence of a pair of counter-rotating streamwise vortices during the ejection process. To overcome the defect of the conditional sampling technique with a detector probe, Guezennec et al. (1989) devised an asymmetry-preserving averaging scheme with the quadrant technique; they obtained a solitary vortices picture that more closely resembles the instantaneous one observed in instantaneous flow fields given by direct numerical simulations (Kim et al., 1987). Asymmetry of instantaneous structures in the turbulent boundary layer has also been investigated by Robinson et al. (1989). However, this feature of coherent structures has never been derived directly experimentally from velocity measurements by probes such as hotwires and LDV. It is obvious that these direct numerical simulations without turbulent models have only been made at moderate Reynolds numbers (from 10^4 to 10^5), and the large-scale coherent structures in the field-scale flows cannot be investigated by this method because the Reynolds number in the field is too large. Turbulent phenomena such as the rapid rolling-up of sediment on a seabed as well as boils in flood river flows have not been made clear. Understanding the features of the coherent structures in the field is an important topic for engineering applications.

In the present study, the authors attempted to apply a new experimental method to reconstruct a quasi-instantaneous image of coherent structures from velocity data obtained experimentally using a multi-point simultaneous measurement system (Meng et al., 1990).

2. Experimental equipment and method of data sampling

2.1. Wind tunnel

The experiments on the coherent structure of turbulence in a reciprocating oscillatory flow have been performed in a wind tunnel 14 m long with a rectangular cross-section of

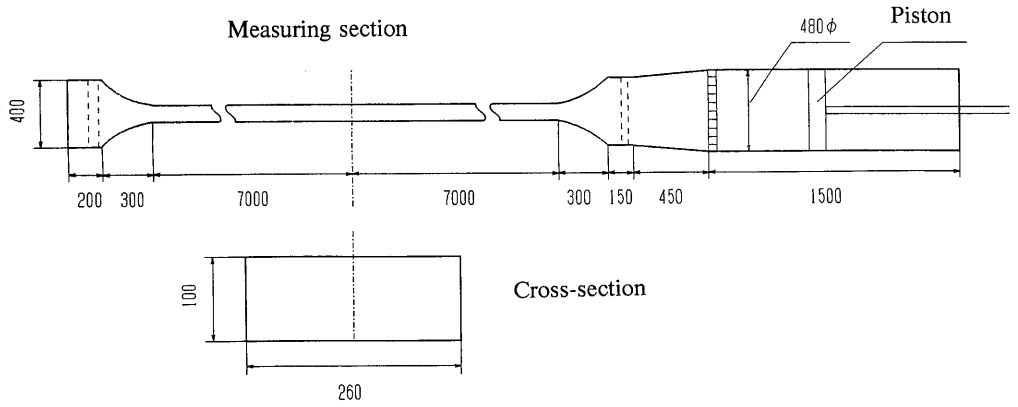

Fig. 1. Experimental apparatus.

26 cm × 10 cm (fig. 1). The details of the wind tunnel are described in a previous paper (Hino et al., 1983). The origin of the coordinate system is located at the center of the channel bottom, X, Y, and Z being taken in the mean flow direction, in the direction normal to the channel bottom and in the direction perpendicular to the X–Y plane, respectively.

The experimental conditions were the same as those for the previous paper (Hino et al., 1990). The amplitude of the cross-sectional mean velocity U was 2.57 m/s, and the period of oscillation T was 3.15 s. The Reynolds number, based on the Stokes-layer thickness δ ($= (2\nu/\omega)^{1/2}$ $= 3.87$ mm; ν is the kinematic viscosity, ω is the angular frequency of oscillation), was Re ($= U\delta/\nu$) $= 710$, and the Reynolds number based on the height of wind tunnel d was Re ($= Ud/\nu$) $= 1.84 \times 10^4$. The Stokes parameter $\lambda = d/2\delta$ was 12.9. Coordinates are normalized by using d as the characteristic length.

2.2. Velocity measurement

In this study, the velocity components u–v at a point were measured by X-type constant-temperature anemometers made in our laboratory. The sensors were made of tungsten wire, 5 μm in diameter, and were used at 0.5 overheat ratio throughout this investigation. A frequency response of, typically, greater than 10 kHz was achieved and checked by means of the usual square wave test. The hot-wires were calibrated by means of a laser-Doppler velocimeter equipped with a frequency shifter for use in distinguishing the flow direction. The velocity u as a function of the voltage E out of the hot-wire anemometer was represented by a polynomial

$$u = aE^3 + bE^2 + cE + d, \tag{1}$$

in which constants a, b, c, d were determined by the least-squares method. The outputs of the hot-wires were digitized into 12-bit digits at a sampling frequency of 1 kHz per channel. The analog/digital converter with 24 sample holds employed in this measurement was designed and fabricated in our lab, and it can process a maximum of 24 channels simultaneously. Accordingly, the data on the velocity components u–v at 11 points, which were arranged as indicated in fig. 2, were simultaneously recorded and analyzed by a personal computer (NEC-9801) with 4 MB memory. The layout of the probes and the block diagram of the measurement system are shown in fig. 3.

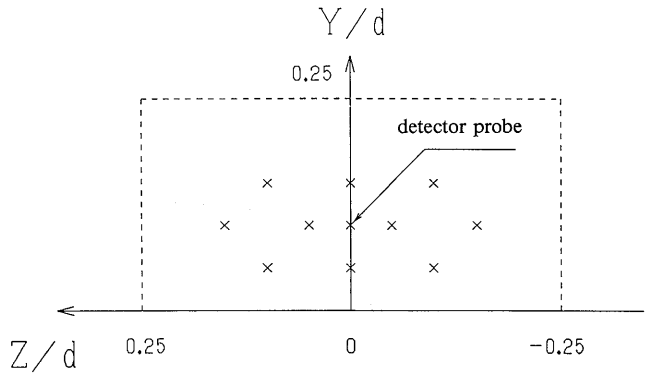

Fig. 2. Arrangement of 11 points for the velocity measurement by X-type hotwires.

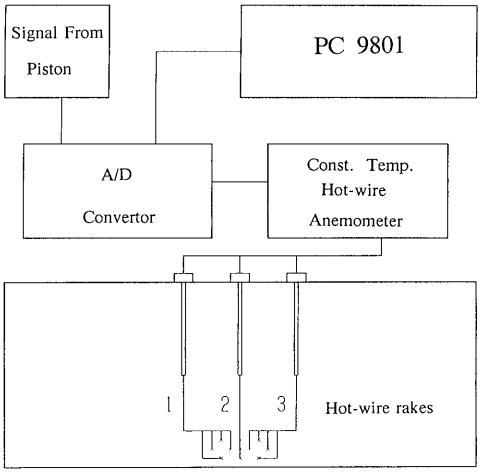

Fig. 3. A block diagram of the measurement system.

2.3. *Conditional sampling*

In order to detect a quasi-instantaneous three-dimensional picture of the coherent structure of turbulence, the quadrant technique proposed by Willmarth and Lu (1972) was adopted. The center probe set at the depth $Y/d = 0.1$ was used as a detector probe, and the remaining ten hot-wire probes were placed to measure the u–v velocity components around it (fig. 2).

In our previous experiments (Hino et al., 1990), we noticed that, in the deceleration phase, most of the high Reynolds stress was produced by ejection type motions; the frequency of appearance of these motions is almost 60 times higher than that of the sweep type motion during the phase $(\frac{9}{18} - \frac{10}{18})\pi$. Hence, this study focussed on the ejection motions. Figure 4 shows sample traces of the data recorded by the detection probe set on the central plane of the wind tunnel. The top trace is the mean flow velocity, which may be considered quasi-steady at a shorter sampling duration although it undergoes unsteady variations for one cycle. The second and third traces are the fluctuating velocity components, u and v, respectively. The bottom one is the variation of the instantaneous Reynolds stress, $-uv$, which indicates an abrupt increase. Data on the fluctuating velocities and mean velocity recorded in the memory saved from 50 ms ahead to 50 ms after the detection, and 100 ms samples were used to obtain one coherent structure. The temporal data were converted to the spatial ones by the Taylor hypothesis of frozen turbulence.

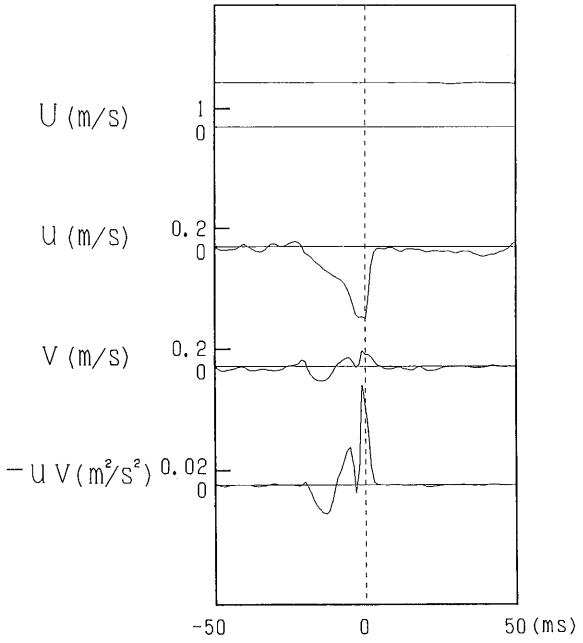

Fig. 4. Simultaneous traces of mean velocity U, velocity fluctuations u, v and the instantaneous Reynolds stress $-uv$ obtained from the detector probe.

3. Estimation method of quasi-instantaneous 3-D image of coherent structure of turbulence from velocity data

A variety of methods for parameter and system identification are available in the field of control engineering and mathematical modelling. These methods are based on the criterion that the mean square of errors at selected data points, between the observed values and those determined from the basic equations describing the system, should be minimized under certain constraints. In our case of a fluid flow, the constraints to be adopted for the optimal estimation may be either the continuity equation or the momentum equations (i.e., the Navier–Stokes equations), or both of these, together with suitable boundary conditions. If both equations are used, the computational effort imposed by the constraint of the momentum equation is formidable, if not impossible. For instance, if the given data points are not sufficient, a computational indeterminacy will arise. Therefore, a simplification is to use only the continuity equation as a constraint for the flow field identification.

In the field of meteorology, only sparse data on wind-velocity distribution over an area are obtainable. For instance, only the ground level wind velocities are measured at more or less randomly distributed observation points. The estimation of the 3-D velocity field over the whole region, which is not necessarily uniform and flat, becomes indispensable, if one is to obtain the initial data for numerical weather prediction or to estimate the time varying velocities for the computation of diffusion of pollutant gases from a factory. To achieve this end, a model called the "MASCON" model or the mass consistent model, has been proposed by Sasaki (1958) and has been further improved and applied to practical problems by, for instance, Sherman (1978).

The applicability of the MASCON model to the estimation of the whole flow field for laboratory-scale flows has been tested, and some improvements made by Hino et al. (1991) for

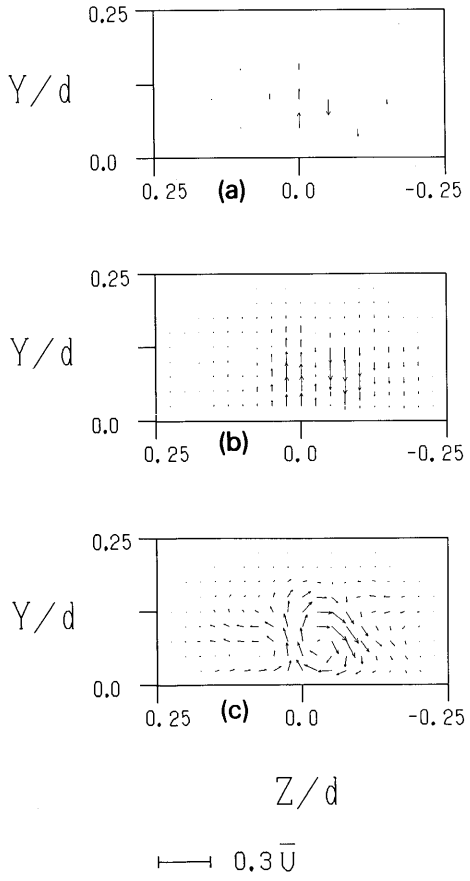

Fig. 5. An example of effectiveness of the new method of data analysis: (a) the velocity vectors measured at 11 points on the (Y–Z) plane; (b) the interpolation of velocities by the "virtual load" method; (c) the final velocity vectors corrected by the "MASCON" model.

both simulation data and wind tunnel data, and a satisfactory degree of success has been achieved.

An example of the effectiveness of the foregoing method is given in fig. 5. The top figure shows the velocity vectors measured at 11 points on the (Y–Z) plane, the middle supplies an interpolation of velocities by the "virtual plate/load" method (Hino et al., 1991), and the bottom figure illustrates the final velocity vectors calculated by using the "MASCON" model; the vortical motion induced by a coherent structure is found clearly.

4. Experimental results and discussion

4.1. Perspective representations of quasi-instantaneous 3-D pictures of coherent structures

From the experimental data obtained by 11 hotwire probes, quasi-instantaneous 3-D pictures of coherent structures can be obtained. Figure 6 shows three sets of contour line graphs of ω_x of coherent structures. The vorticity component ω_x was computed from three-dimensional velocity data estimated by the present method. The contour lines drawn in broken lines show negative vorticity, which means a counter-clockwise motion if viewed from the upstream to the downstream; those drawn in solid lines show the opposite. From the figure, one might be able to

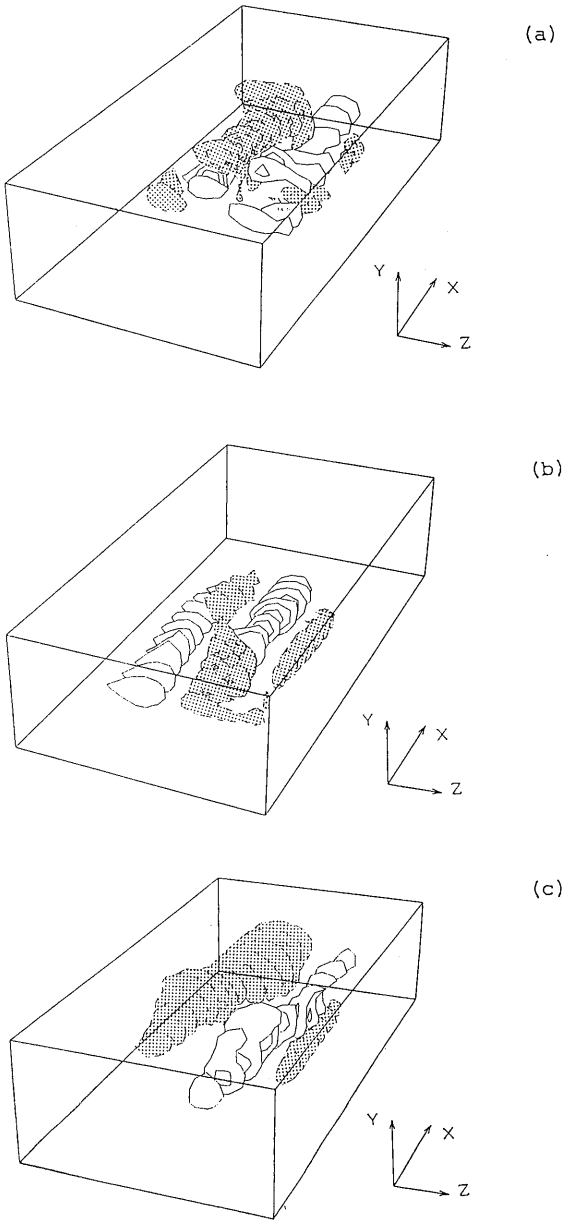

Fig. 6. Perspective view of the contours of vorticity component ω_x: (a) case I; (b) case II; (c) case III.

build a three-dimensional picture of the coherent structure. The orientations of pair eddies are not always regularly aligned, the intensities of twin vortices are not equal, the axes of vortices are usually not straight, and the individual images of the coherent structure differ considerably from each other.

4.2. Raw data to be analyzed

In order to illustrate 3-D configurations of coherent structures, one typical case (case I) will be analyzed in detail. Raw data on hotwire signals taken simultaneously at the 11 sampling points

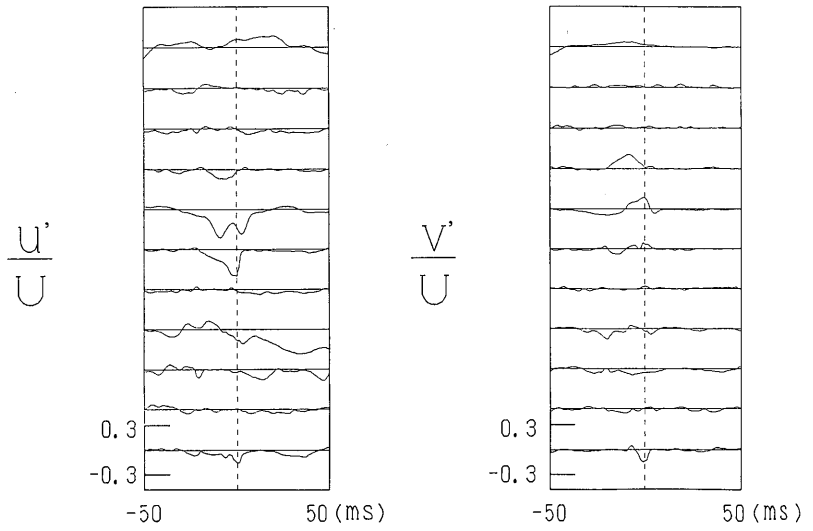

Fig. 7. Raw data on hotwire signals taken simultaneously at the 11 sampling points indicated in fig. 2.

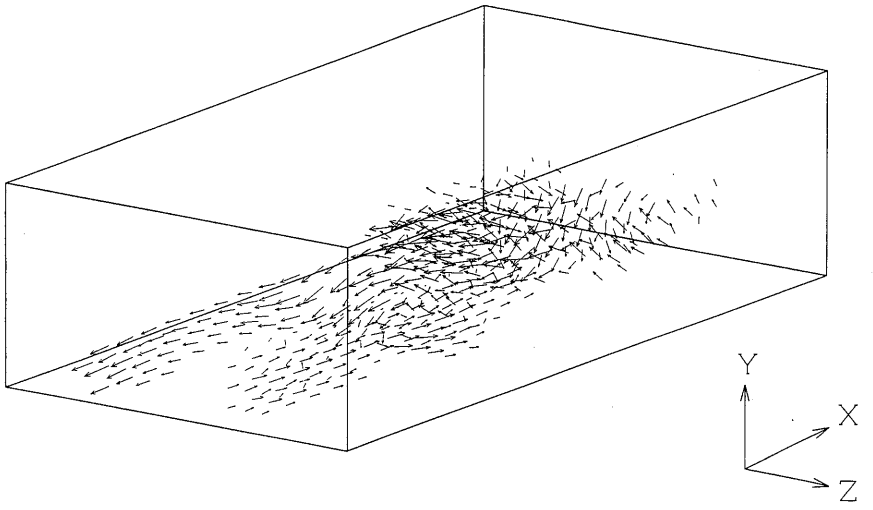

Fig. 8. Bird's eye view of the velocity vector field of the coherent structure of turbulence at phase $\omega t = (\frac{9}{18} - \frac{10}{18})\pi$.

are shown in fig. 7. From these data only, no concrete 3-D image of a coherent structure of turbulence can be obtained. Using the present method, a perspective representation of the fluctuation velocity vectors, which are defined as the deviation from the phase-averaged velocity, can be given in fig. 8. The vectors having an absolute value smaller than 5 percent of the mean velocity were eliminated for clarity. In the central part of the graph, an upward motion of fluid moving at low velocity is dominant, which produces a high Reynolds stress. In contrast, fluid moving at high speed can be seen on the upstream side (left-hand side of the graph) of the low speed fluid. Near the wall and just behind (right-hand side) the central low speed fluid, a whirling motion of fluid is visible.

4.3. Graphs of instantaneous velocity vectors and vorticity contours of the coherent structure

4.3.1. Velocity vectors u, w and vorticity contours of ω_y on (X–Z) planes

Figures 9 and 10 show, respectively, the velocity-fluctuation vector fields of (u, w) and vorticity contours of ω_y in various (X–Z) planes. In fig. 9, the arrows in the central part are directed toward the left, indicating that the flow there is low-speed relative to the mean flow. A rotating flow can be found in the positive Z side. In order to describe the configuration of the coherent structure, the vorticity, ω_y. has been computed from the velocity components u and w. The solid lines in fig. 10 are contours of positive value of ω_y vorticity, and broken lines are negative ones. A positive value of ω_y means a counter-clockwise rotation, and vice versa. It can be noticed that the centers of vorticity patches are aligned in an asymmetrical position. All the analyses of the remaining data which are not cited in this paper show the asymmetry of coherent structure.

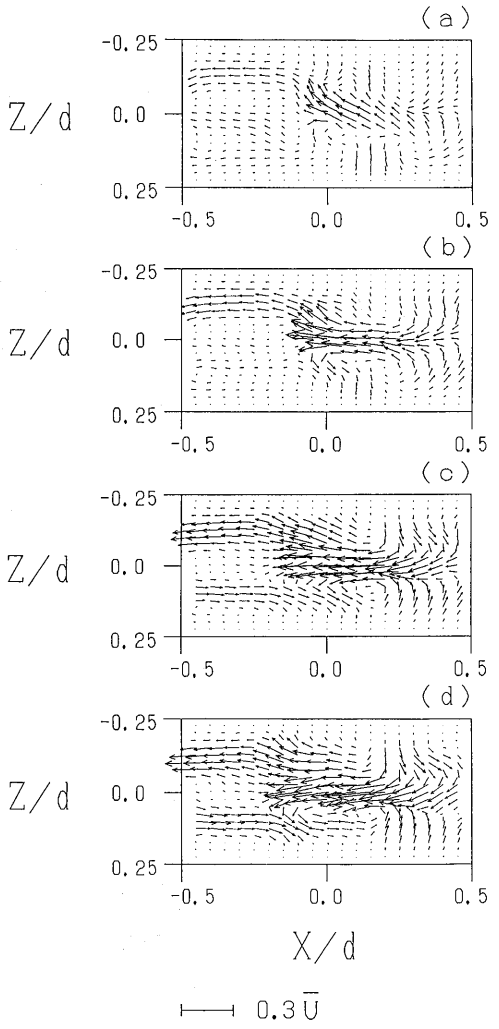

Fig. 9. Velocity vectors of (u, w) in the various (X–Z) planes: (a) $Y/d = 0.125$; (b) $Y/d = 0.100$; (c) $Y/d = 0.050$; (d) $Y/d = 0.025$.

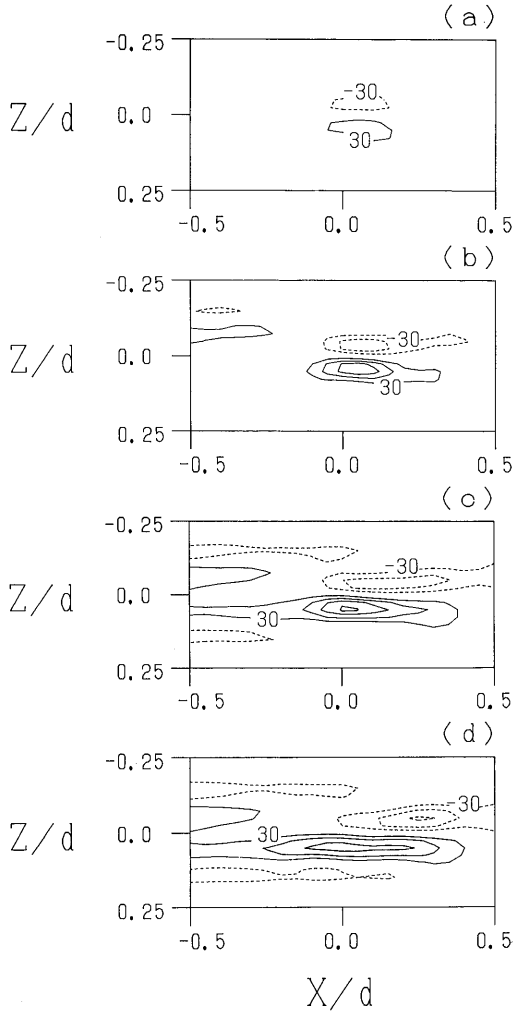

Fig. 10. Contours of ω_y in the various (X–Z) planes: (a) $Y/d = 0.125$; (b) $Y/d = 0.100$; (c) $Y/d = 0.050$; (d) $Y/d = 0.025$. (The contours are in an increment of $30\,s^{-1}$.)

4.3.2. Velocity vectors, v, w and vorticity contours of ω_x on (Y–Z) planes

Figures 11 and 12 illustrate, respectively, the velocity-fluctuation vector fields of v and w and the contour maps of ω_x in various (Y–Z) planes seen from the downstream direction. The velocity vectors (fig. 11) reveal that the coherent structure is rotating motions and the vorticity component ω_x of this structure (fig. 12) is a double deck; i.e., a pair of weaker rotating motions is located beneath a pair of stronger counter-rotating motions. This feature is quite different from that of the ensemble-averaged one, and is qualitatively in agreement with the longitudinal vortex found in the transition process of boundary-layers by Williams et al. (1984). In this case, the vortices in the upstream side are weaker and the distance between two vortices is wider, but in the downstream side they become stronger and the distance between them becomes narrower. Figures 10 and 12 indicate clearly that the coherent structure is associated with the instantaneous three-dimensional vorticity field. The strong upward flow detected at $X/d = 0$ and $Y/d = 0.1$ is caused by this vortical structure.

4.3.3. Veloity vectors u, v and vorticity contours of ω_z on (X–Y) planes

Figures 13 and 14 show, respectively, the velocity-fluctuation vectors (u, v) and vorticity maps of ω_z on a vertical plane parallel to the mean flow direction. The arrows in the (X–Y) plane at $Z/d = 0$ (fig. 13c) are directed upward to the left, indicating that the low-speed flow moves away from the bottom; in contrast, the arrows at the $Z/d = 0.2$ section (fig. 13e) point downward to the right, which indicates that the high-speed flow moves in the downstream direction relative to the mean velocity. Figure 14c shows that a strong negative vorticity ω_z exists at the $y/d = 0.125$ location away from the wall. Considering that the phase-averaged mean $\overline{\omega_z}$ at the phase of $(\frac{9}{18} - \frac{10}{18})\,\pi$ is negative and has the minimum value at the wall, the vertical profile of $\overline{\omega_z} + \omega_z$ has

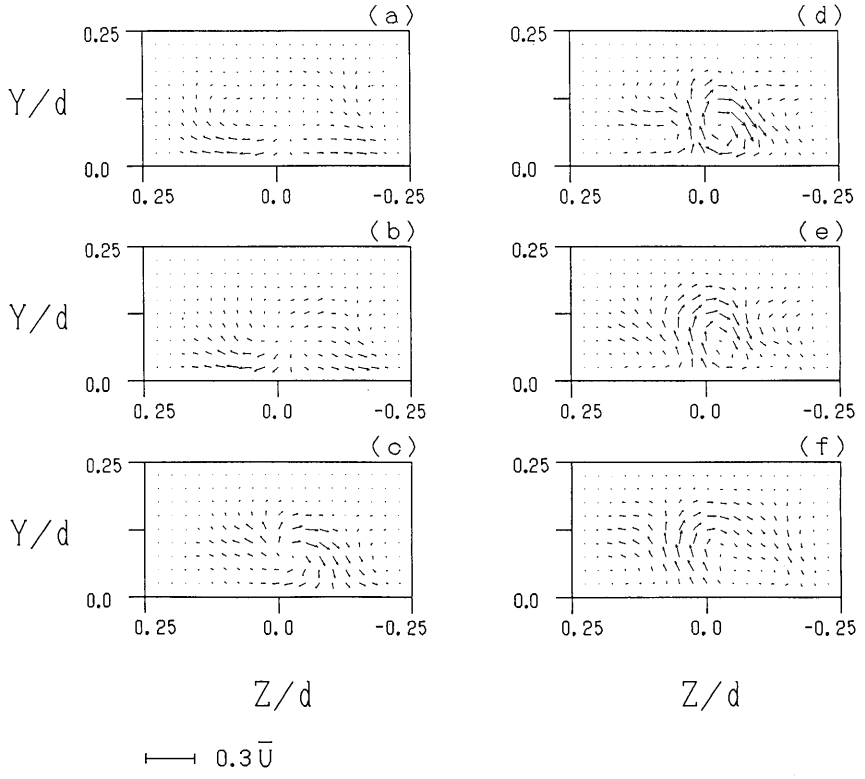

Fig. 11. Velocity vectors of (v, w) in the various (Y–Z) planes: (a) $X/d = -0.15$; (b) $X/d = -0.10$; (c) $X/d = -0.05$; (d) $X/d = 0$; (e) $X/d = 0.05$; (f) $X/d = 0.10$.

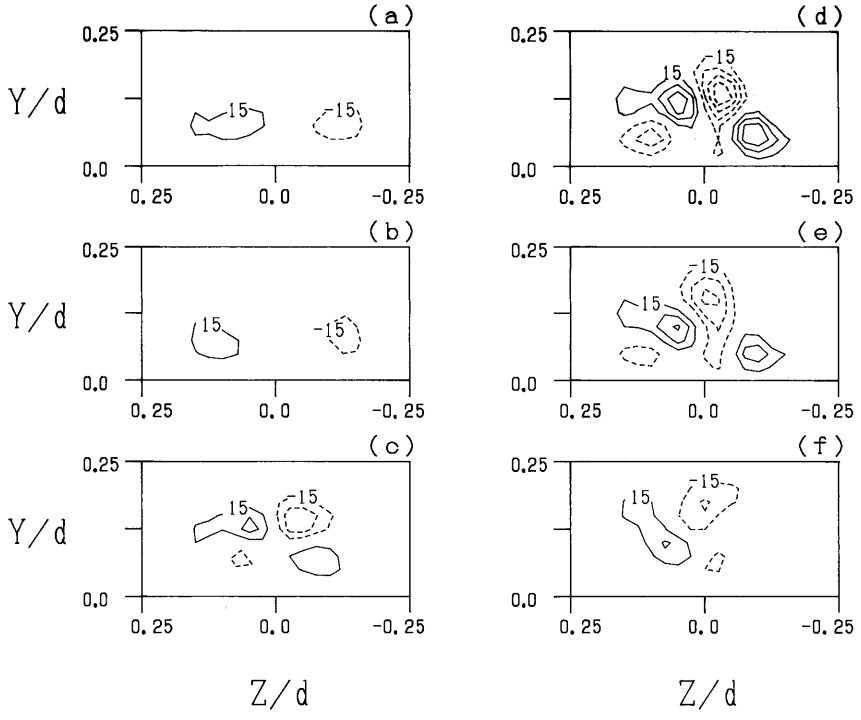

Fig. 12. Contours of ω_x in the various (Y–Z) planes: (a) $X/d = -0.15$; (b) $X/d = -0.10$; (c) $X/d = -0.05$; (d) $X/d = 0$; (e) $X/d = 0.05$; (f) $X/d = 0.10$. (The contours are in an increment of 15 s^{-1}.)

a peak in the region with the strong negative vorticity ω_z, which indicates that a higher-shear layer is created there. From figs. 12 and 14, we can see that the high-shear layer is above the vortex loop associated with the vorticity ω_x. This concept was envisaged by Williams et al. (1984). Figure 15 illustrates the vertical profiles of instantaneous velocity $U + u$ of the coherent structure in the (X–Y) plane at $Z/d = 0$. The formation of an internal shear layer is clearly shown in the figure.

4.4. Flow-visualization on computer – Timeline and streakline representations of flow patterns

Since a complete set of velocity components of the flow around a coherent structure has been estimated by use of the present technique, flow patterns caused by the coherent structure of turbulence can be illustrated through computer simulation of timelines. The timelines are drawn by the tracer lines discharged successively at a short interval from a vertical line perpendicular to the wall or from a horizontal line parallel to the wall. The temporal variation of the trajectory of a tracer particle released at time t_0 from the origin x_0, $X(t; x_0, t_0)$, is expressed by

$$\mathrm{d}X/\mathrm{d}t = V(X, t), \tag{2}$$

where $V(X, t)$ means the velocity vector at position X and time t. Equation (2) has been numerically integrated, based on the assumption that the coherent structure is frozen.

This procedure is similar to the flow visualization technique using hydrogen bubbles. It was the method applied effectively to investigate the transition from laminar to turbulent flow by Hama and Nutant (1963) and the coherent motion by Kline et al. (1967). Figure 16 gives time lines obtained from the fluid motion of the coherent structure, which resembles closely those in direct

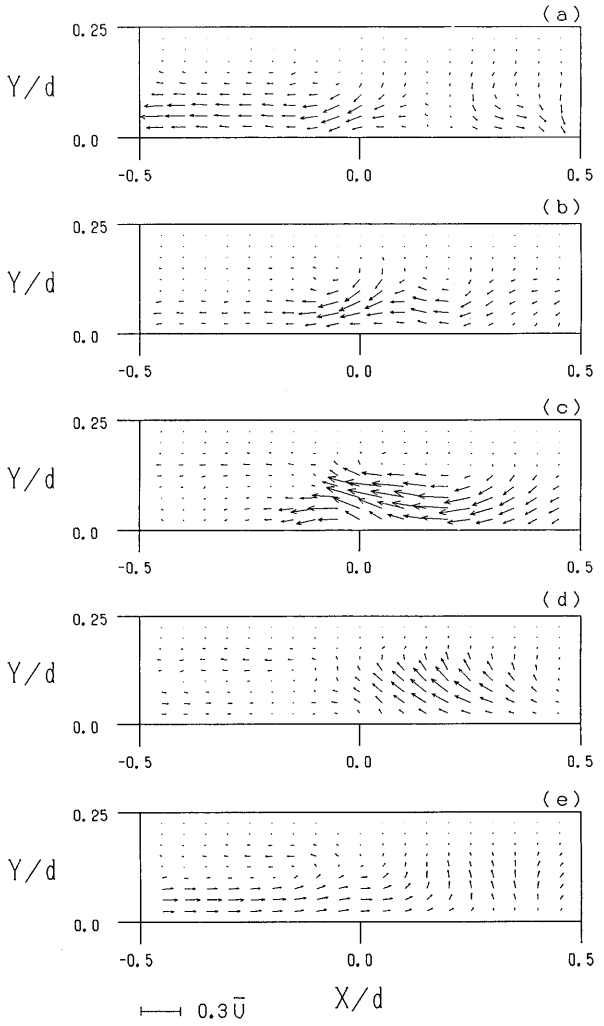

Fig. 13. Velocity vectors of (u, v) in the various $(X-Y)$ planes: (a) $Z/d = -0.2$; (b) $Z/d = -0.1$; (c) $Z/d = 0.0$; (d) $Z/d = 0.1$; (e) $Z/d = 0.2$.

numerical simulation by Kim et al. (1987) on the coherent structures in the fully developed turbulent boundary layer. The coherent motion causes tracer particles of time lines to blow up violently. The swirling motion of the tracer particles in fig. 16b is induced by the vortical motion shown in fig. 11. Figure 17 shows the perspective view of horizontal timelines released from the horizontal line parallel to the wall. The distortion of horizontal timelines is due to the low-speed fluid motion existing in the central parts, as shown in fig. 9. By the same procedure, a streakline representation of the coherent structure is drawn in fig. 18.

4.5. Ensemble-averaged picture

In order to elucidate how the instantaneous (non-ensemble-averaged) image of coherent structures differs from the ensemble-averged one, an ensemble-averaged picture is derived from 20 sampling data sets. Figures 19 and 20 illustrate the ensemble-averaged vectors and the

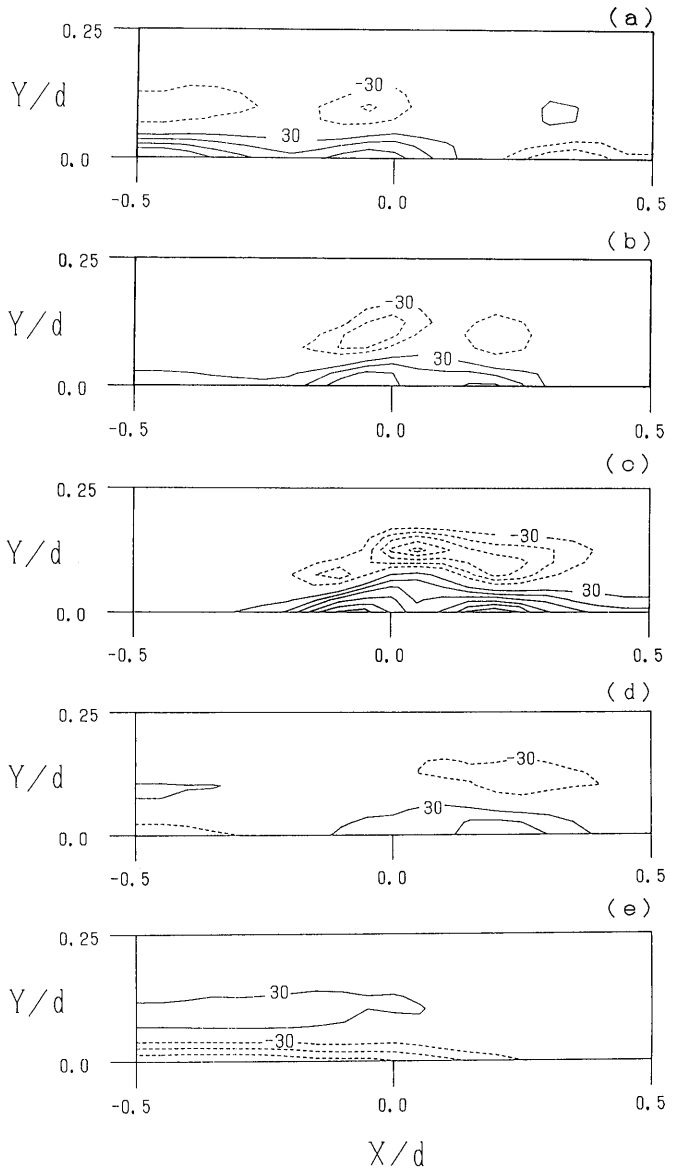

Fig. 14. Contours of ω_z' in the various $(X-Y)$ planes: (a) $Z/d = -0.2$; (b) $Z/d = -0.1$; (c) $Z/d = 0.0$; (d) $Z/d = 0.1$; (e) $Z/d = 0.2$. (The contours are in an increment of $30\ s^{-1}$.)

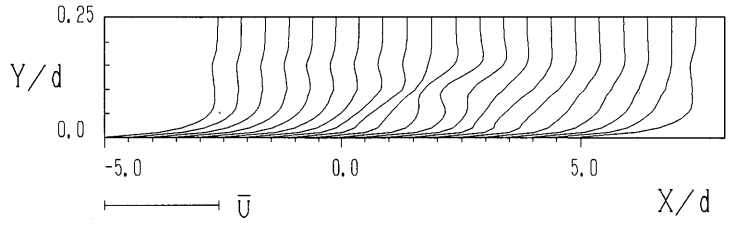

Fig. 15. Vertical profiles of quasi-instantaneous velocity $U + u$ at the plane $Z/d = 0$.

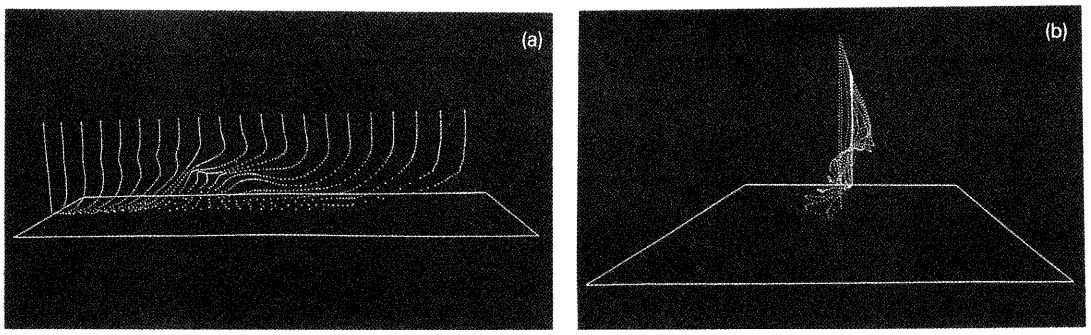

Fig. 16. Perspective view of time-lines released from the vertical line perpendicular to the wall: (a) side view; (b) view from the downstream direction.

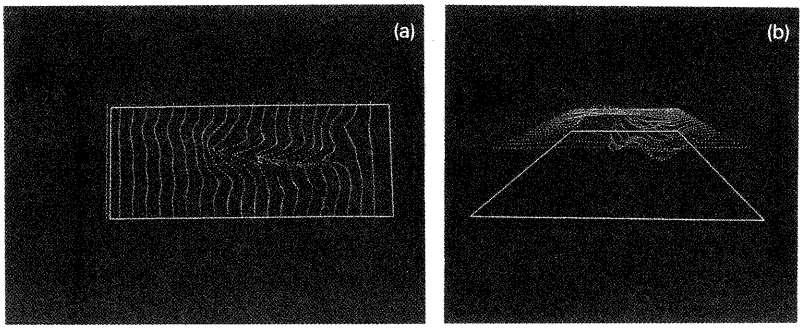

Fig. 17. Perspective view of time-lines which released from the horizontal line parallel to the wall: (a) top view; (b) view from the downstream direction.

vorticity contours; i.e., (u, w) and ω_y on the $(X–Z)$ plane parallel to the wall at the height of $Y/d = 0.1$, and (v, w) and ω_x on the $(Y–Z)$ plane normal to the mean flow direction at the origin $X/d = 0$, respectively. Although the contour lines shown in these figures are not completely symmetric about the central plane because of the scarcity of data, they lead to the same conclusion, as discussed by various authors (e.g., Fukunishi and Sato, 1987a, b; Hino et al., 1990): that the coherent structure is invoked by a pair of symmetrical vortices, that is, a counter-rotating fluid motion, inclined and elongated in the downstream direction.

A comparison of figs. 19 and 20 with figs. 9–14 clearly shows differences between the ensemble-averaged picture and the instantaneous image: (1) paired vortices are not necessarily symmetric, i.e., one may be somewhat ahead or behind the other; (2) the ensemble-averaged picture obtained by the hotwires shows a vortical structure elongated in the downstream direction, in contrast to the instantaneous one; (3) the coherent structure derived from the instantaneous analysis shows a double-decked structure, which is quite different from those given by ensemble average.

5. Conclusions

From this study, the following conclusions were obtained.

(1) A quasi-instantaneous three-dimensional image of coherent structures of turbulence was first reconstructed directly from sparse experimental data on velocities by using a new method of

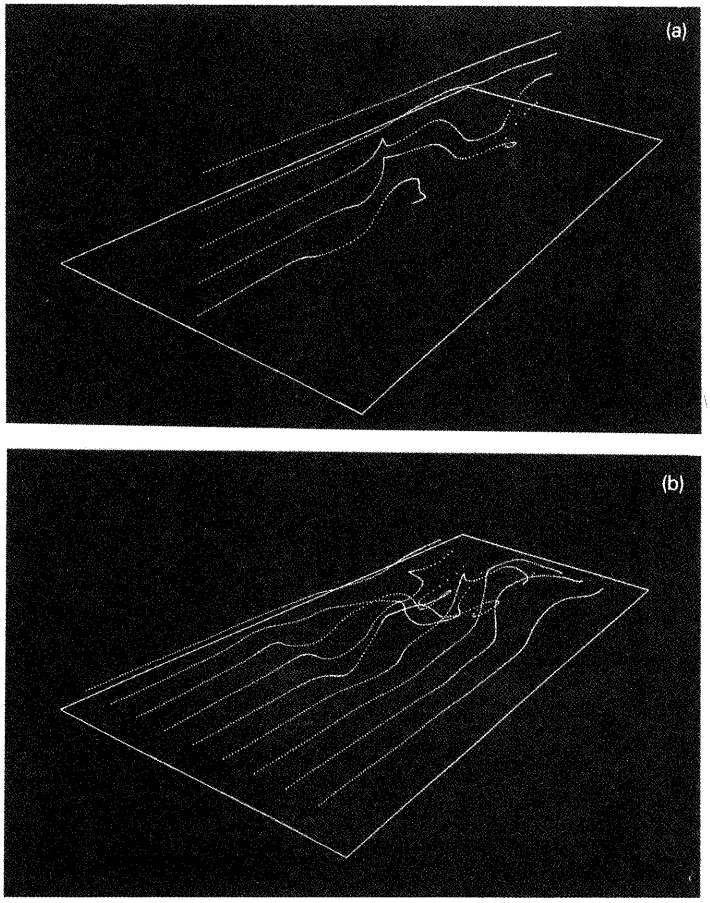

Fig. 18. Perspective view of streak lines: (a) tracers are released from the vertical line; (b) tracers are released from the horizontal line.

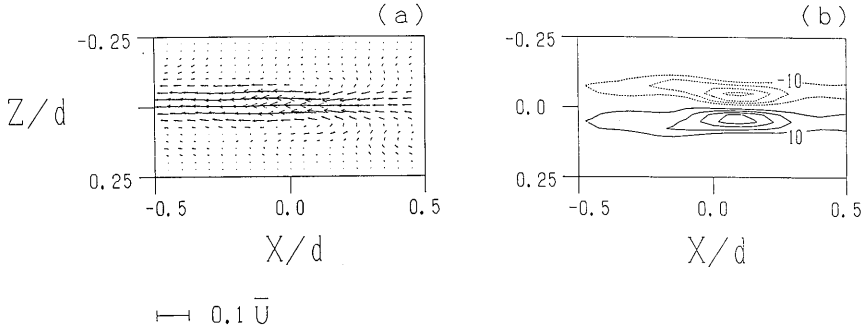

Fig. 19. Ensemble-averaged (u, w) vectors and contours of vorticity component ω_y in $(X–Z)$ planes at the height of $Y/d = 0.10$: (a) ensemble-averaged (u, w) vectors; (b) contours of vorticity component ω_y computed from the ensemble-averaged data. (The contours are in an increment of $10\,s^{-1}$.)

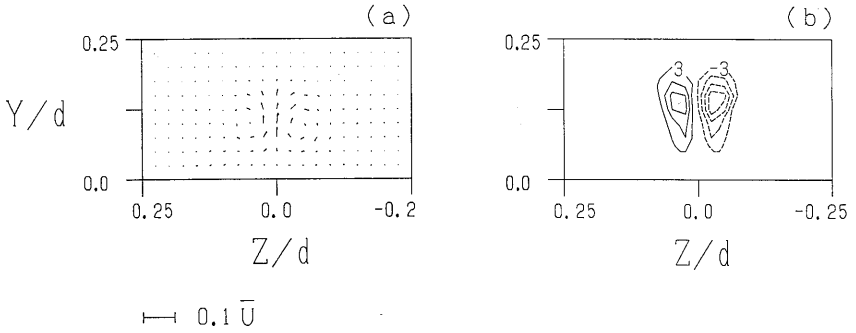

Fig. 20. Ensemble-averaged (v, w) vectors are contours of vorticity component ω_x in $(Y\text{–}Z)$ planes in the section of $X/d = 0$: (a) ensemble-averaged (v, w) vectors; (b) contours of vorticity component ω_x computed from the ensemble-averaged data. (The contours are in an increment of $3\,s^{-1}$.)

data analysis. The results derived by this method do not contradict, and almost coincide with, the already available knowledge obtained from the conditional averaging method and the numerical simulation.

We considered that this method is powerful for the study of turbulence structures in the field-scale flows at very high Reynolds numbers ($Re = 2.4 \times 10^6$, Hino et al., 1992).

(2) The quasi-instantaneous coherent structure is quite different from the ensemble-averaged one, composed of an asymmetric pair of counter-rotating fluid motions.

(3) Flow patterns induced by the coherent structure were clarified by the flow visualization technique on a computer, using the velocity data obained by the present method.

Acknowledgement

The authors would like to acknowledge the laborious cooperative work in data sampling performed by Mr. M. Murayama, Master course student in our department.

References

Antonia, R.A. and D.K. Bisset (1989) Three-dimensional aspects of the organized motion in a turbulent boundary layer, O. Metais and M. Lesieur eds, *Turbulence and Coherent Structures*, 141–157.

Blackwelder, R.F. and R.E. Kaplan (1976) On the wall structure of the turbulent boundary layer, *J. Fluid Mech. 76*, 89–112.

Fukunishi, Y. and H. Sato (1987a) Formation of intermittent region by coherent motions in the turbulent boundary layer, *Fluid Dyn. Res. 2*, 113–124.

Fukunishi, Y. and H. Sato (1987b) Study of developing process of coherent structures in the turbulent boundary layer, *AIAA 19th Fluid Dynamics.*

Guezennec, Y.G., U. Piomelli and J. Kim (1989) On the shape and dynamics of wall structures in turbulent channel flow, *Phys. Fluid A 1(4)*, 52–58.

Hama, F.R. (1962) Streaklines in a perturbed shear flow, *Phys. Fluids 5*, 644–650.

Hama, F.R. and J. Nutant (1963) Detailed flow-field observation in the transition process in a thick boundary layer, *Proc. 1963 Heat Transfer and Fluid Mechanics Inst.* (Stanford University Press) 77.

Hino, M., M. Kashiwayanagi, A. Nakayama and T. Hara (1983) Experiments on the turbulence statistics and the structure of a reciprocating oscillatory flow, *J. Fluid Mech. 131*, 363–400.

Hino, M., Y. Fukunishi and Y. Meng (1990) Experimental study of three dimensional large-scale structure in a reciprocating oscillatory flow, *Fluid Dyn. Res. 6*, 261–275.

Hino, M., Y. Meng and M. Murayama (1991) An attempt at estimating the instantaneous velocity field of a nonstationary flow from velocity measurement at a few points, *Fluid Dyn. Res. 7*, 101–108.

Hino, M., Y. Meng and N. Murayama (1992) Field measurements on the 3D large-scale turbulent structures in the flood flow by multi-channel simultaneous measuring system, *Proc. of Hydraulic Eng., JSCE 36*, 175–180, (in Japanese).

Kim, J. (1985) Turbulence structures associated with the bursting event, *Phys. Fluid 28(1)*, 52–58.

Kim, J., P. Moin and R.D. Moser (1987) Turbulence statistics in fully developed channel flow at low Reynolds number, *J. Fluid Mech. 177*, 133–166.

Kline, S.J. and P. W. Runstadler (1959) Some preliminary results of visual studies of the flow model of the wall layers of the turbulent boundary layer, *J. Appl. Mech., Trans. ASME (ser. E) 2*, 166.

Kline, S.J., W.C. Reynolds, F.A. Schraub and P.W. Runstadler (1967) The structure of turbulent boundary layers, *J. Fluid Mech. 30*, 741–773.

Meng, Y., M. Murayama and M. Hino (1990) Measurements of the whole instantaneous image of the large-scale structure in a reciprocating oscillatory turbulent flow, *Proc. 22nd Conf. on Turbulence, Japan Soc. Fluid, Mech.*, (in Japanese), 312–317.

Moin, P. and J. Kim (1982) Numerical investigation of turbulent channel flow, *J. Fluid Mech. 118*, 341–377.

Robinson, S.K., S.J. Kline and P.R. Spalart (1989) A review of quasi-coherent structures in a numerically simulated turbulent boundary layer, NASA TM-102191.

Robinson, S.K. (1991) Coherent motions in the turbulent boundary layer, *Ann. Rev. Fluid Mech. 23*, 601–639.

Sasaki, Y. (1958) An objective analysis based on the variational method, *J. Meteor. Soc. Japan. 36*, 77–88.

Sherman, C.A. (1978) A mass-consistent model for wind fields over complex terrain, *J. Appl. Meteor. 17*, 312–319.

Williams, D.R., H. Fasel and F.R. Hama (1984) Experimental determination of the three-dimensional vorticity field in the boundary-layer transition process, *J. Fluid Mech. 149*, 179–203.

Willmarth, W.W. and S.S. Lu (1972) Structure of the Reynolds stress near the wall, *J. Fluid Mech. 55*, 65–92.